International Journal of Mass Spectrometry 300 (2011) 91–98

Contents lists available at ScienceDirect

International Journal of Mass Spectrometry

journal homepage: www.elsevier.com/locate/ijms

Vibrational predissociation spectroscopy of the H_2-tagged mono- and dicarboxylate anions of dodecanedioic acid

Michael Z. Kamrath, Rachael A. Relph, Timothy L. Guasco, Christopher M. Leavitt, Mark A. Johnson*

Sterling Chemistry Laboratory, Yale University, P.O. Box 208107, New Haven, CT 06520, United States

ARTICLE INFO

Article history:
Received 15 September 2010
Received in revised form 7 October 2010
Accepted 14 October 2010
Available online 21 October 2010

Keywords:
Cryogenic ion trap
Mass spectrometry
Infrared spectroscopy
Hydrogen bonding
Electrospray

ABSTRACT

Vibrational predissociation spectroscopy of the $HOOC(CH_2)_{10}COO^-$ and $^-OOC(CH_2)_{10}COO^-$ anions is carried out by predissociation of weakly bound H_2 molecules. The $HOOC(CH_2)_{10}COO^-$ $(H_2)_2$ and $^-OOC(CH_2)_{10}COO^-$ $(H_2)_{10}$ cluster ions are formed by H_2 attachment to the electrospray-generated bare ions in an ion trap cooled to below 20 K using a closed cycle helium cryostat. The photofragmentation behavior indicates that the H_2 binding energy is about 600 cm^{-1}, which is similar in strength to that found in Ar-tagged ions. The spectra indicate that the monoanion adopts a cyclic structure through the formation of an asymmetrical, internal anionic H-bond.

1. Introduction

Vibrational spectroscopy is emerging as an important tool in the structural characterization of macromolecular ions generated using electrospray ionization (ESI). This is evidenced by the explosion of papers reporting isomer analysis by comparison of vibrational action spectra obtained by infrared multiphoton dissociation (IRMPD) with predictions from electronic structure calculations [1–6]. There are, however, complications in this strategy because the intrinsic non-linearity of the IRMPD method obscures direct comparison with the harmonic absorption spectrum that is readily computed using commercial software packages [7]. Moreover, the fluxional nature of the molecules gives rise to many isomers at low temperature which can often interconvert under ambient conditions [8]. A powerful way to overcome these limitations is through the use of so-called "messenger spectroscopy" [9,10], where the ion of interest is complexed with a weakly bound ligand (such as a rare gas atom), and the vibrational action spectrum is monitored by photoinduced loss of the messenger. In this approach, the ion is intrinsically cooled to an upper limit defined by the ligand binding energy, and efficient intramolecular vibrational energy redistribution upon excitation in the fingerprint region of the infrared leads to prompt ejection of the messenger. The resulting action spectra are linear in laser intensity, with a few notable exceptions [11], and therefore more accurately reflect the linear absorption profiles associated with specific local minimum structures of the target molecule or cluster. This method has been widely used to study ions and ion–solvent clusters that can be prepared using supersonic jet technology [10,12–29]. On the other hand, application of this method to the classes of ions that can only be generated with alternative techniques such as ESI or laser vaporization is still in its infancy, with a notable recent paper reporting spectra of He or Kr tagging in a temperature controlled ion trap subsequent to ion generation [6,30].

Here we present vibrational predissociation spectra of the anions generated from sequential deprotonation of dodecanedioic acid using H_2 as a messenger, where we exploit the recent demonstration by Wang et al. [31,32] that large numbers of H_2 molecules (up to 12) can be efficiently attached to multiply charged ions from an ESI source using a 10 K radio-frequency (RF) quadrupole ion trap. This is significant because H_2 is often non-reactive and quite weakly bound to a variety of closed-shell molecular ions prepared by ESI, and was, in fact, one of the species used in 1980s for the first reports of the messenger technique [10,21,22]. In the case of $H_5O_2^+$, for example, the binding energy and perturbation induced by H_2 were on the same order as that found for Ar tagging [21,33]. In this paper, we extend the trap-based methods to singly charged anions by pulsing the H_2/He mixture into the trap, and report the resulting vibrational spectra of the $HOOC(CH_2)_{10}COO^-$ and $^-OOC(CH_2)_{10}COO^-$ ions over the range 800–4300 cm^{-1}. These data are interpreted in the context of a closed, H-bonded ring form for the singly charged species, an arrangement that was inferred by Woo et al. [34] from their analysis of the photoelectron spectrum of this species.

* Corresponding author. Tel.: +1 203 432 5226; fax: +1 203 432 6144.
E-mail address: mark.johnson@yale.edu (M.A. Johnson).

1387-3806/$ – see front matter © 2010 Elsevier B.V. All rights reserved.
doi:10.1016/j.ijms.2010.10.021

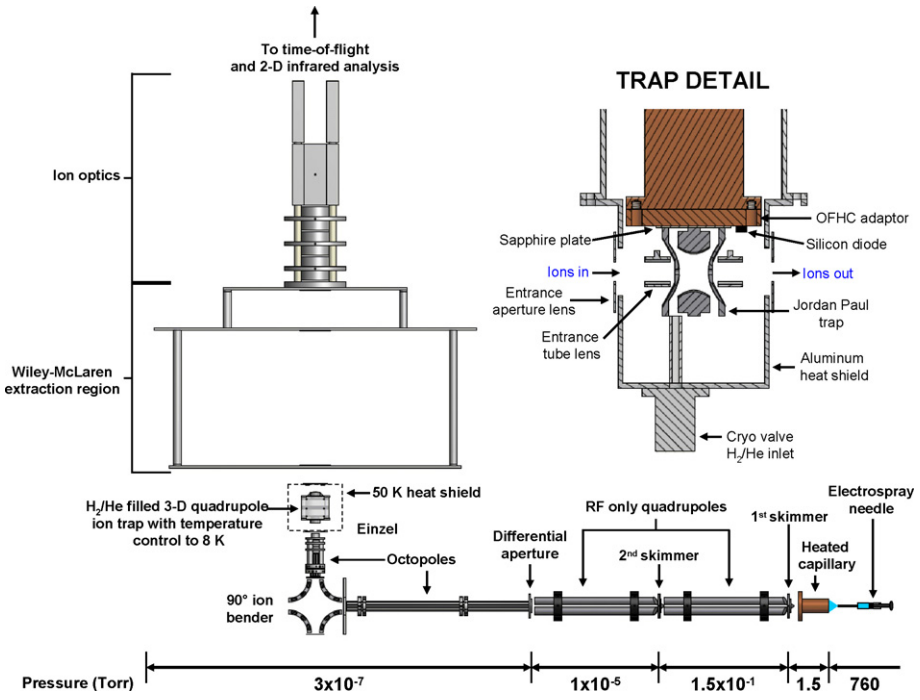

Fig. 1. Schematic diagram (to scale) of the ESI ion source interfaced to the cold RF ion trap and time-of-flight (TOF) mass spectrometer. The ESI-generated ions are guided through two differentially pumped stages by two RF only quadrupoles to a differential aperture leading into the final vacuum envelope. Octopole ion guides and a 90° turning quadrupole deflector direct the beam to a series of focusing elements before injection into the cryogenically cooled Paul trap, where ions are collisionally cooled and tagged with H_2 (see trap detail). Upon ejection from the trap, ions are allowed to drift into the main extraction region before coaxial acceleration focuses them at the laser interaction region of the tandem TOF photofragmentation spectrometer.

2. Experimental details

2.1. H_2 tagging in the quadrupole trap with pulsed buffer gas

A schematic diagram of the recently completed instrument at Yale is displayed in Fig. 1. The time-of-flight (TOF) photofragmentation part of the apparatus, which has been described in detail elsewhere [35,36], has been fitted with a new ESI ion source designed closely after the scheme demonstrated by Wang and Wang [31]. In the present study, anions are produced through electrospray ionization of a ~0.5 mM solution of dodecanedioic acid in an 80/20 solution of methanol and water. The ions are extracted from the electrospray using standard differential pumping techniques, where the first stage (1.5 Torr) involves passing the ions through a heated 0.76 mm diameter capillary (5 cm in length, $T = 65\,^{\circ}C$) followed by two more stages (150 mTorr and 3×10^{-4} Torr, respectively) separated by two 1.5 mm skimmers. After leaving the first skimmer, the ions are guided through the second by custom RF only quadrupoles leading to the final differential aperture (1.5 mm) into the main vacuum envelope, held at a base pressure of 3×10^{-7} Torr. The RF voltage was supplied using the circuit recommended by O'Connor and co-workers [37,38]. Once inside the main chamber, the beam is guided by an RF octopole to a DC turning quadrupole, which rejects the neutral background, followed by another RF octopole leading to the ion lenses that interface the ion beam to the trap. The key element is the injection of the ESI generated ions into a low temperature (minimum temperature is 8 K) Paul trap (Jordan), where the ions are stored for a carefully controlled time interval prior to being ejected by applying a low voltage pulse (60 V) to one of the trap electrodes. The ejected ions drift into the Wiley–McLaren extraction region of the existing TOF instrument in a coaxial arrangement. Because the ions drift with relatively high kinetic energy into this region, the TOF performance is somewhat degraded, resulting in somewhat broadened mass peaks with asymmetrical peak shapes. Once inside, two high voltage pulses accelerate them to a final energy of 3.5 keV, and bring them to a transient focus at the laser interaction region located about 1.5 m from the source.

The trap is cooled with a closed cycle He cryostat (Sumitomo, 1.5 W at 4.2 K) and filled with a burst of gas (20% H_2 in He) using a pulsed valve (Parker Series 9) mounted on the 50 K heat shield on the outside of the trap housing (see trap detail in Fig. 1). The gas is introduced directly into the trap through a 3.9 mm ID tube that is 3.4 cm long. The trap is mounted to the cold head by an 8.5 mm thick adapter made of oxygen free high purity copper (OFHC) and a 1 mm thick sapphire plate which provides electrical insulation. Indium foil (0.1 mm) is placed between these junctions to maximize thermal conductivity. The silicon diode temperature probe (Lake Shore: D6008610) is placed on the bottom of the OFHC adapter as indicated in Fig. 1 (trap detail). The valve is pulsed on for 10 ms with a 15 V square pulse (10 Hz), where the backing pressure is sufficiently low to avoid hydrodynamic flow into the trap. While the exact pressure rise and temperature profile of the buffer gas in the trap are difficult to determine, optimum operation occurs when the He/H_2 pulse raises the ambient pressure in the chamber by about 5×10^{-7} Torr. Note that the aperture from the trap to the main chamber is about 3 mm, while the chamber is evacuated with a 2000 L/s diffusion pump (Edwards Diffstak 250).

The performance of the cold Paul trap as a medium for attaching H_2 has been documented in the earlier report by Wang and co-workers [31]. That work, however, was carried out with a continuous stream of gas introduced to the trap. It is therefore useful to present the role of the timing sequence in the generation of $^{-}OOC(CH_2)_{10}COO^{-}\ (H_2)_n$ complexes, which is displayed in the series of mass spectra shown in Fig. 2. The set of sharp peaks toward higher mass are consistent with H_2 addition to the $^{12}C_{12}H_{20}O_4{}^{2-}$ isotopologue, while the small shoulder on the high mass side of the parent peak (denoted by * in trace a) as well as the interlopers in the dominant distribution of higher mass peaks are consistent with the presence of the $^{13}C^{12}C_{11}H_{20}O_4{}^{2-}$ isotopologue. The lat-

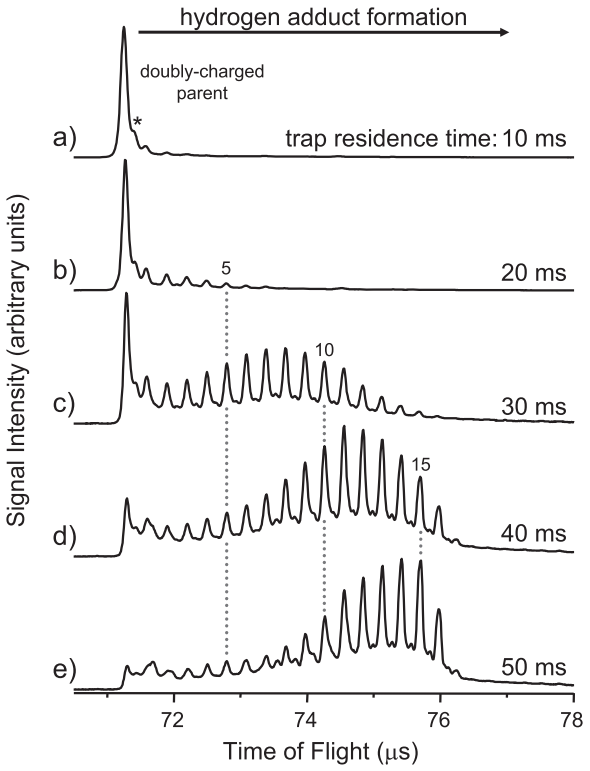

Fig. 2. Mass spectra demonstrating the effect of trap residence time on H_2 tagging efficiency. The doubly charged parent ion ($^-OOC(CH_2)_{10}COO^-$, at left) is observed to accumulate increasing numbers of H_2 molecules as the residence time is lengthened from (a) 10 ms to (e) 50 ms.

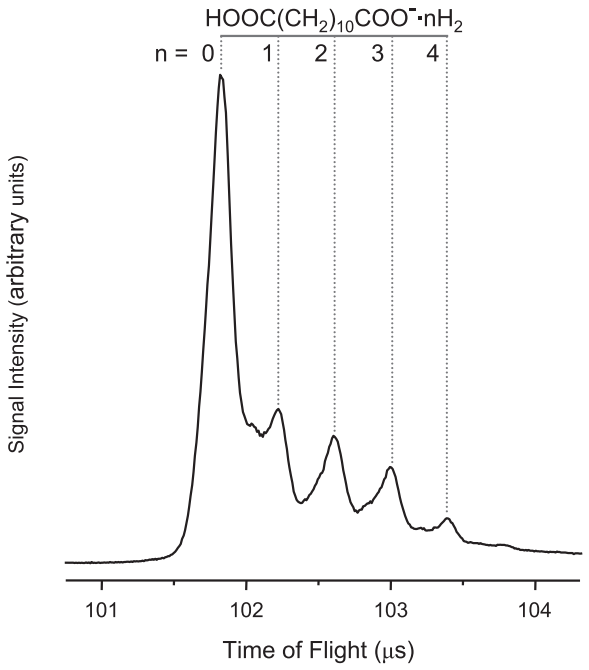

Fig. 3. Mass spectrum of $HOOC(CH_2)_{10}COO^-(H_2)_n$, $n = 1$–4, illustrating the addition of H_2 molecules to the singly charged species.

ter is calculated to occur with 13.5% of the dominant isotopologue given the 1.1% natural abundance of ^{13}C. Interestingly, the growth of the adducts is dramatically dependent on the trap extraction delay time, and continues to evolve toward larger sizes quite late in the cycle before stabilizing at around 40 ms. This induction time appears to reflect the balance between having sufficiently high pressure in the trap to stop the ions, allow cooling of both the ions and the buffer gas, as well as enable the three-body collisions required for association to occur. The residual pressure in the cell must also be minimized at the time of extraction so that the ions are not destroyed by collision-induced dissociation (CID). It is significant that this can be accomplished given the large driving forces at play in a quadrupole trap (as opposed to the commonly used 22-pole [39–41], for example). Not surprisingly, condensation requires careful adjustment of the RF voltage and injection energy to minimize collisional heating. Note that the mass ratio of the trapped ions to that of the dominant buffer (He) is about 50, providing a favorable scenario for cooling with minimal translational heating from the drift field. While this scenario is likely not conducive to accurate temperature control of the ions processed in this manner, the application for messenger spectroscopy does not require this feature, and it is straightforward to attach large numbers of H_2 molecules to the dianion.

Because the pulsed introduction of the buffer gas used here differs from the continuous scheme employed in the first report of H_2 condensation [31], we also explored the possibility of adding H_2 to the singly charged $HOOC(CH_2)_{10}COO^-$ ion. This is a significant test as only the doubly charged system was discussed in that work, suggesting that the adducts were more difficult to form on the singly charged system. Fig. 3 presents the results for the $HOOC(CH_2)_{10}COO^-$ anion, and while the extent of solvation is clearly reduced, formation of clusters with up to four H_2 molecules are readily observed. This successful tagging of the singly charged anion is quite useful in this study as it provides an excellent opportunity to explore the detailed structural differences between mono- and dianions by comparing their vibrational spectra.

2.2. Spectroscopic protocols

Vibrational predissociation spectra were obtained for both the singly and doubly charged species by monitoring the evaporative loss of H_2 molecules upon resonant excitation [9,10]:

$$X^{q-} \cdot (H_2)_n + h\nu \rightarrow X^{q-} \cdot (H_2)_m + (n-m)H_2 \quad (1)$$

Photoexcitation between 2350 and 4300 cm^{-1} was carried out using a pulsed, (~7-ns pulse width, 10 Hz) Nd:YAG pumped OPO/OPA laser (LaserVision). The lower-energy range (800–2300 cm^{-1}), was generated by parametric mixing of the 3 and 1.5 μm beams in $AgGaSe_2$ [42,43]. The spectra were recorded in the linear action regime determined by following the fluence-dependence of the photodissociation yield, and the raw photofragment signal was normalized for fluctuations in laser pulse energy over the scan. This procedure is necessary to correct for very large changes in output energy of the laser, especially in the lower energy region, but we note that there are still complications in quantitatively comparing the action spectra with the calculated linear absorption spectra due to intrinsic changes in the laser divergence properties over the scan range.

2.3. Computational details

DFT calculations were carried out using the Gaussian 03 package of programs [7]. Geometry optimizations and harmonic frequency calculations of the $^-OOC(CH_2)_{10}COO^-$, $^-OOC(CH_2)_{10}COO^-$ H_2 and $HOOC(CH_2)_{10}COO^-$ ions were carried out using the B3LYP functional and the 6-311++G(d,p) basis set. All harmonic frequency calculations were scaled by 0.956 to bring the calculated C–H stretching fundamentals into agreement with those observed in experimental vibrational spectrum of the dianion. This value is in line with other commonly used scaling factors [44].

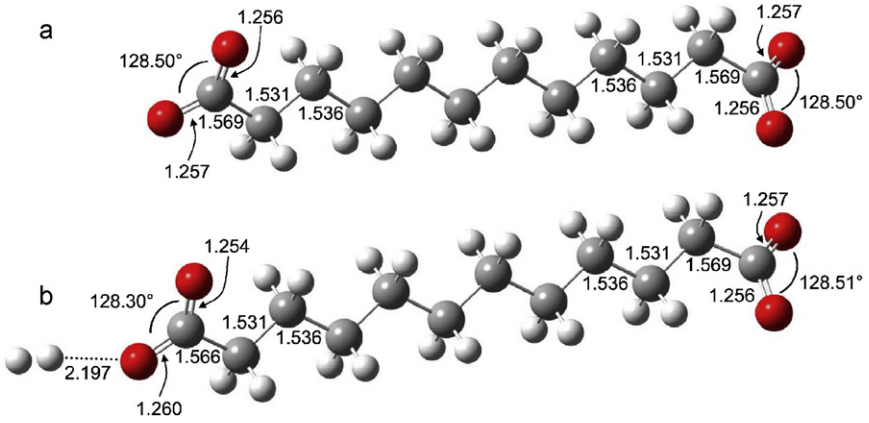

Fig. 4. Optimized geometries of (a) $^{-}OOC(CH_2)_{10}COO^{-}$ and (b) $^{-}OOC(CH_2)_{10}COO^{-}$ H_2 using the B3LYP functional in conjunction with the 6-311++G(d,p) basis set; selected bond lengths are indicated in angstroms. Note that the addition of H_2 causes only minor perturbation of this system (e.g. C=O bond length increases by ~0.003 Å).

3. Results and discussion

3.1. Vibrational predissociation spectra of the $^{-}OOC(CH_2)_{10}COO^{-}(H_2)_{10}$ ion

The implementation of H_2 tagging for vibrational spectroscopy obviously requires that H_2 attachment does not significantly perturb the intrinsic spectrum of the target ion. To explore this effect, we carried out electronic structure calculations of the binary $^{-}OOC(CH_2)_{10}COO^{-}$ H_2 complex to identify the binding site of, and perturbation induced by H_2, with the results presented in Fig. 4a and b for the bare ion and the adduct, respectively. Interestingly, H_2 attaches to one of the carboxylate groups where the excess charge is concentrated. The H_2 tag has the advantage that, unlike the situation with rare gas tagging, it effectively "reports" on the degree of perturbation through the changes in its characteristic frequency [13,21]. The vibrational mode of the H_2 moiety in the binary complex is calculated (at the harmonic level) to redshift about 250 cm^{-1} relative to the free H_2 band, with a concomitant enhancement of the nominally forbidden infrared transition. Comparison of the structures in Fig. 4, however, indicates that H_2 indeed does not significantly perturb the equilibrium geometry of the dianion, with bond lengths changing at most by 0.003 Å and the O–C–O angles by less than 0.5°. Here we are primarily concerned with the perturbation of the vibrational spectrum, and the harmonic spectra of the bare ion and the single hydrogen adduct are presented in Fig. 5a and b, respectively, with a comparison of the experimental and calculated frequencies presented in Table 1. The addition of a single H_2 molecule produces slightly nonequivalent CO_2 groups, resulting in the calculated frequencies of the two symmetric and asymmetric CO_2 stretches to be split by ~5 cm^{-1}, considerably smaller than the ~20 cm^{-1} perturbation experimen-

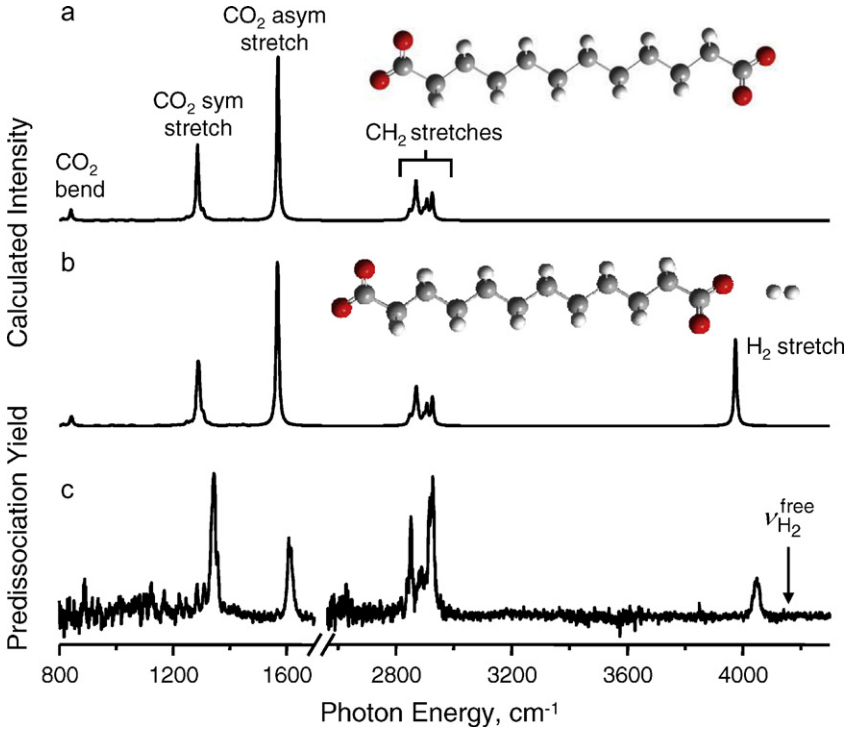

Fig. 5. Calculated harmonic spectra (B3LYP/6-311++G(d,p)) of (a) $^{-}OOC(CH_2)_{10}COO^{-}$ and (b) $^{-}OOC(CH_2)_{10}COO^{-}$ H_2. Calculated frequencies have been scaled by 0.956 as described in the text. The vibrational predissociation spectrum of (c) $^{-}OOC(CH_2)_{10}COO^{-}$ $(H_2)_{10}$ was obtained by monitoring the loss of 5 H_2 molecules for excitation in the region 2550–4300 cm^{-1} whereas the loss of 3 H_2 channel was isolated for detection of absorption in the 800–1700 cm^{-1} portion of the spectrum. The frequency of the isolated H_2 stretch at 4158 cm^{-1} is indicated by the arrow in (c).

Table 1
Comparison of the experimentally measured vibrational transitions of $^{-}OOC(CH_2)_{10}COO^{-}$ $(H_2)_{10}$ with calculated harmonic frequencies for $^{-}OOC(CH_2)_{10}COO^{-}$, $^{-}OOC(CH_2)_{10}COO^{-}$ H_2 and H_2.

Method	Species	Frequencies, cm^{-1}				
		CO_2 bend	CO_2 sym. stretch	CO_2 asym. stretch	CH stretches	H_2 stretch
Experimental	$^{-}OOC(CH_2)_{10}COO^{-}$ $(H_2)_{10}$	890	1345	1611	2840, 2853, 2887, 2917, 2929	4046
Calculated[a]	$^{-}OOC(CH_2)_{10}COO^{-}$ (H_2)	840, 844	1286, 1289	1568, 1571	2847, 2850, 2867, 2872, 2896, 2907, 2926	3974
	$^{-}OOC(CH_2)_{10}COO^{-}$	840	1286	1571	2847, 2867, 2871, 2896, 2907, 2926	N/A
	H_2	N/A	N/A	N/A	N/A	4224

[a] Calculated at the B3LYP/6-311++G(d,p) level and scaled by 0.956.

tally observed upon complexation of one CO_2 group with H_2O [30].

The abundance pattern observed for the dianion in Fig. 2d displays a maximum yield at around $n = 10$, prompting us to carry out the predissociation survey at this cluster size. The dominant photofragment observed upon resonant excitation of the highest energy CH stretching band at 2929 cm^{-1} corresponded to the loss of 5 H_2 molecules. This behavior is quite similar to that found for the Ar clusters of many ions, where the extent of the fragmentation is controlled by sequential unimolecular dissociation within the ansatz of an evaporative ensemble [45,46]. The similarity in photofragmentation properties between Ar and H_2 thus indicates that the H_2 dissociation energy is also in the neighborhood of 600 cm^{-1}. The $n = 10$ parent was selected for the present study because it is prepared in abundance, and the loss of 3–5 H_2 molecules is readily observed in the second (reflectron) stage of mass selection (as opposed to loss of a single H_2, for example, from the mono-adduct).

The H_2 predissociation spectrum of the $n = 10$ complex is presented in Fig. 5c. The high energy region was detected via the loss of 5 H_2 channel, while the lower energy region was monitored by following the loss of 3 H_2, as anticipated from the binding energy estimate of about 600 cm^{-1} per H_2 dissociation. The limited resolution in the secondary (reflectron) TOF analysis stage was actually advantageous in the present experiment as many adjacent loss channels (e.g. $n = 4$–6) could be monitored within the same detection window, thus minimizing complications arising from specific channel dependence of the action spectra. The perturbation-induced H_2 feature appears centered at 4046 cm^{-1}, 112 cm^{-1} to the red of the band origin in the bare molecule [47], and is interestingly one of the broader features in the spectrum. The shift is, however, even less than the calculated ~250 cm^{-1} value, strongly supporting the suggestion that hydrogen plays an effective role as a messenger to accurately report the spectrum of the ion to which it is attached. The bands associated with the dianion appear at lower energy, and result from the C–H stretches near 2900 cm^{-1}, the CO_2 stretches next near 1500 cm^{-1} and the CO_2 bending mode at 890 cm^{-1}. The locations of these features are quite similar to those found in the Kr-tagged suberate dianion [30]. The band contours are consistent with the exclusive formation of the all-*trans* isomer depicted in Fig. 4a, (see Supplementary data for other calculated structures) which was identified as the lowest energy form in the photoelectron work of Wang and co-workers on the closely related tetradecanedioic acid dianion [32]; the all-*trans* motif was also identified as the form of the parent ion in the vibrational spectroscopy study of the suberate system [30].

The CO_2 bands are readily assigned to the symmetric and asymmetric stretches at 1345 cm^{-1} and 1611 cm^{-1}, respectively, which appear close to the predicted locations, but have relative intensities opposite to that anticipated from the harmonic calculation (Fig. 5a and b). Note that with an even distribution of the H_2 molecules attached to each carboxylate (*vide infra*), the solvent will not break the symmetry of the dianion as was the case in the binary adduct, $^{-}OOC(CH_2)_{10}COO^{-}$ H_2. The residual splitting between the two close doublets is quite small in the symmetrical ion, and would not be resolved with the present instrumental resolution of about 2 cm^{-1}. In this case, we expect that the four bands derived from the collective in- and out-of-phase motions on each CO_2 center will be dominated by the out-of-phase components. Bands derived from the C–H stretches are more complex and appear as a multiplet with clearly distinguishable interlopers on the low energy side of each strong peak. The lowest energy band at 890 cm^{-1} is traced to a mode with dominant contributions from displacements along the O–C–O bend and C–C stretching coordinates, as pointed out earlier by Asmis and co-workers [30].

The fine structure of the C–H feature is of interest as calculations reveal that it is composed of many closely spaced transitions roughly derived from the symmetric and asymmetric stretches of each contributing methylene group, thus forming a pseudo band structure as this motion delocalizes over the backbone of the aliphatic carbon chain. As a general rule, the collective modes based on the symmetric C–H stretch appear lower in energy and primarily contribute to the peak at 2853 cm^{-1} in the experimental spectrum, while the higher energy features near 2929 cm^{-1} mostly involve the asymmetric stretches. Single transitions contributing most of the intensity are often traced to the CH_2 groups closer to the carboxylates and therefore reflect the proximity of the boundary inherent in this finite chain.

Finally, we note that the H_2 band centered at 4046 cm^{-1} appears as a nearly symmetrical feature. Given the substantial redshift of the band relative to that in bare H_2, one might have anticipated that, with 10 H_2 molecules attached, those closest to the carboxylate oxygens would exhibit the largest shifts, with more remote sites gradually shifting back toward the unperturbed position [48]. The fact that the observed band is homogeneous suggests that many H_2 molecules are accommodated in the first solvation shell around each ionic center, and the sharp drop-off at $n = 16$ displayed in Fig. 2e would be consistent with each shell consisting of eight H_2 molecules. To gauge the likely packing scenario at play, we carried out a calculation (B3LYP/6-311++G(d,p)) of the simpler $CH_3CO_2^{-}$ $(H_2)_8$ cluster, with a minimum energy structure reproduced in Fig. 6. Note that 8 H_2 molecules form a large shell with the H_2 molecules standing off almost equidistant from the ion, accounting for the relatively narrow feature in the spectrum. A key aspect of this structure is that the H_2 molecules are oriented with their intermolecular axes pointing roughly along the electric field lines emanating from the excess charge center. Such an arrangement would appear to optimize the pairwise electrostatic interaction to the ion, thus placing the H_2 molecules in an unfavorable relative configuration for their mutual attraction.

3.2. Vibrational predissociation spectrum of $HOOC(CH_2)_{10}COO^{-}$ $(H_2)_2$

Because the H_2 molecules are not efficiently attached to the singly charged anion, we selected the $n = 2$ parent for the spectroscopic survey to optimize parent intensity and the degree of mass-loss upon photoexcitation, which is especially difficult

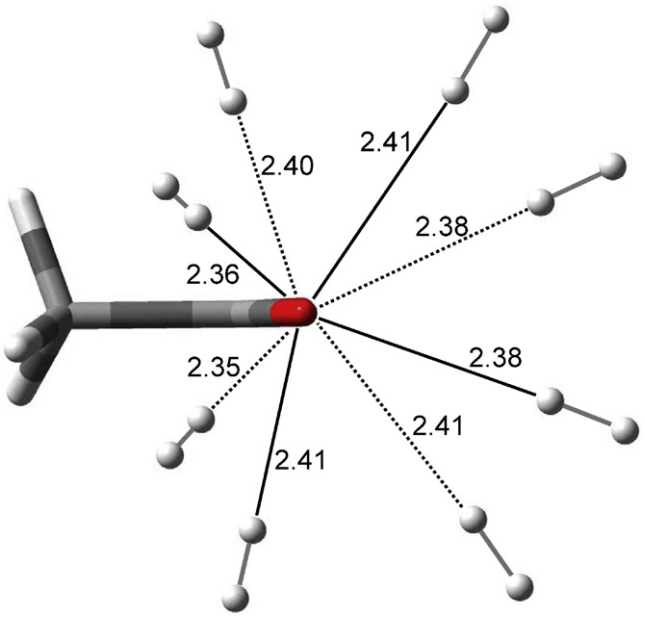

Fig. 6. Optimized geometry of the acetate ion solvated by 8 H_2 molecules, $CH_3COO^-(H_2)_8$, calculated at the B3LYP/6-311++G(d,p) level of theory. The carboxylate group is surrounded by H_2 molecules oriented with their intermolecular axes pointed along the lines originating from each oxygen atom in the carboxylate group. The bond lengths (Å) are indicated in the figure. All of the H_2 bond lengths are roughly 0.75 Å, and the solid lines connect to the visible oxygen while the dashed lines originate from the eclipsed oxygen.

if only one H_2 is lost. The predissociation spectrum of the $HOOC(CH_2)_{10}COO^-(H_2)_2$ parent is presented in Fig. 7b, which was detected throughout by monitoring the loss of both H_2 molecules. Experimental and calculated band positions are collected in Table 2. The H_2 stretch is again clear at the blue edge of the spectrum, but it is interestingly blue-shifted (by 47 cm^{-1}) compared to the corresponding band in the dianion complex, bringing it closer to the transition in bare H_2. One aspect of the experimental spectrum that is quite clear is that it does not display any features in the vicinity of the free OH, the tell-tale band indicating the presence of the linear isomer with the calculated spectrum found in Fig. 7d. While the absence of a free OH could conceivably result from inefficient energy transfer to the H_2 tag from the remote location of the OH group, we note that the previous photoelectron study [34] also concluded that the cyclic form was the only species present in the ion ensemble. In addition, we note that our calculations predict the cyclic form to be more stable than the linear isomer by over 6500 cm^{-1}. We therefore proceed to discuss the observed band patterns in the context of the cyclic isomer shown in the inset in Fig. 7c. For example, the formation of the cyclic isomer provides a compelling rationalization for the significant reduction of the redshift displayed by the H_2 molecule attached to this species. Specifically, it is reasonable to anticipate that the intramolecular H-bond will concentrate the excess charge on the tethered oxygen atoms, thus reducing the electrostatic perturbation on the H_2 ligands, which in turn yields an H_2 frequency closer to that of the bare molecule.

At a qualitative level, it is clear that the low energy (1000–1800 cm^{-1}) bands in the monoanion (Fig. 7b) are much more complex than those displayed by the dianion (Fig. 7a). This is anticipated by the harmonic spectrum of the cyclic isomer presented in Fig. 7c, but we note that the strongest calculated band near 2300 cm^{-1}, which corresponds to the parallel vibration of the shared proton, is not evident in the experimental spectrum. This is not surprising, however, as the features associated with the bridging proton vibrations are often quite anharmonic [49], and typically appear strongly mixed with nearby vibrational modes nominally associated with the flanking molecular structures.

Because of the complexity associated with disentangling the features directly resulting from oscillation of the shared proton, it is useful to consider how the intramolecular proton bond affects the bands arising from the two carboxylate functionalities effectively linked by the bridging proton. In particular, the structure in Fig. 7c indicates that the ring closes in an asymmetrical fashion such that the bridging proton is located much closer to one of the oxygen atoms (calculated separations are 1.029 and 1.540 Å, respectively). The 2.556 Å calculated distance between the two oxygen atoms bound by the proton is nonetheless quite short, so that the system conforms to a low-barrier H-bond reminiscent of analogous ring structures recently studied by Morton and co-workers. [50]

Perhaps the best indication of the asymmetry in the H-bond can be extracted from behavior of the C=O stretches, which appear relatively isolated in the spectrum near 1600 and 1800 cm^{-1}. In the case of the open structure, we would expect to find relatively unperturbed bands associated with the carboxylate moiety (such as those in Fig. 7a), as well as with the neutral carboxylic acid. The latter bands are typically near 1800 cm^{-1} for the C=O stretch and 1200 cm^{-1} for the C–OH stretch, with these asymptotic positions indicated by the arrows in Fig. 7b. The spectrum of the monoanion indeed displays two strong bands in the high energy region expected for the C–O stretches, with one of them falling in essentially the same location as that found for the asymmetric CO_2 stretch in the dianion (arrows in Fig. 7a). A higher energy feature emerges in the monoanion however, at 1721 cm^{-1}, which falls about 70 cm^{-1} below the expected position for the isolated acid functionality. The asymmetrical intramolecular H-bond in the cyclic motif provides a compelling rationalization for this red-shift, as such behavior would be expected for the C=O nominally on the acid constituent as its proton is partially donated to the carboxylate embedded along the edge of the cyclic structure. We also note that the features assigned to the higher energy C–O stretches in the monoanion appear degraded toward lower energy while those in the open dianion are quite sharp. This effect is likely associated with the mechanics of a strained ring, where the stretching frequencies are highly sensitive to small changes in the intermolecular H-bond. While beyond the scope of this first report, this behavior calls for further study of the monoanions, perhaps exploring the spectral evolution with chain length.

Table 2
Comparison of the experimentally measured vibrational transitions of $HOOC(CH_2)_{10}COO^-(H_2)_2$ with calculated harmonic frequencies of the ring and chain isomers of $HOOC(CH_2)_{10}COO^-$ and H_2.

Method	Species	Frequencies, cm^{-1}					
		CO_2 asym. stretch	C=O stretch	Shared proton	CH stretches	OH stretch	H_2 stretch
Experimental	$HOOC(CH_2)_{10}COO^-(H_2)_2$	1608	1721	~1950	2846, 2858, 2889, 2920		4093
Calculated[a]	$HOOC(CH_2)_{10}COO^-$ ring	1568	1673	2513	2854, 2870, 2876, 2886, 2928, 2933, 2952	N/A	N/A
	$HOOC(CH_2)_{10}COO^-$ chain	1578	1731	N/A	2872, 2901, 2911, 2926, 2940	3596	N/A
	H_2	N/A	N/A	N/A	N/A	N/A	4224

[a] Calculated at the B3LYP/6-311++G(d,p) level and scaled by 0.956.

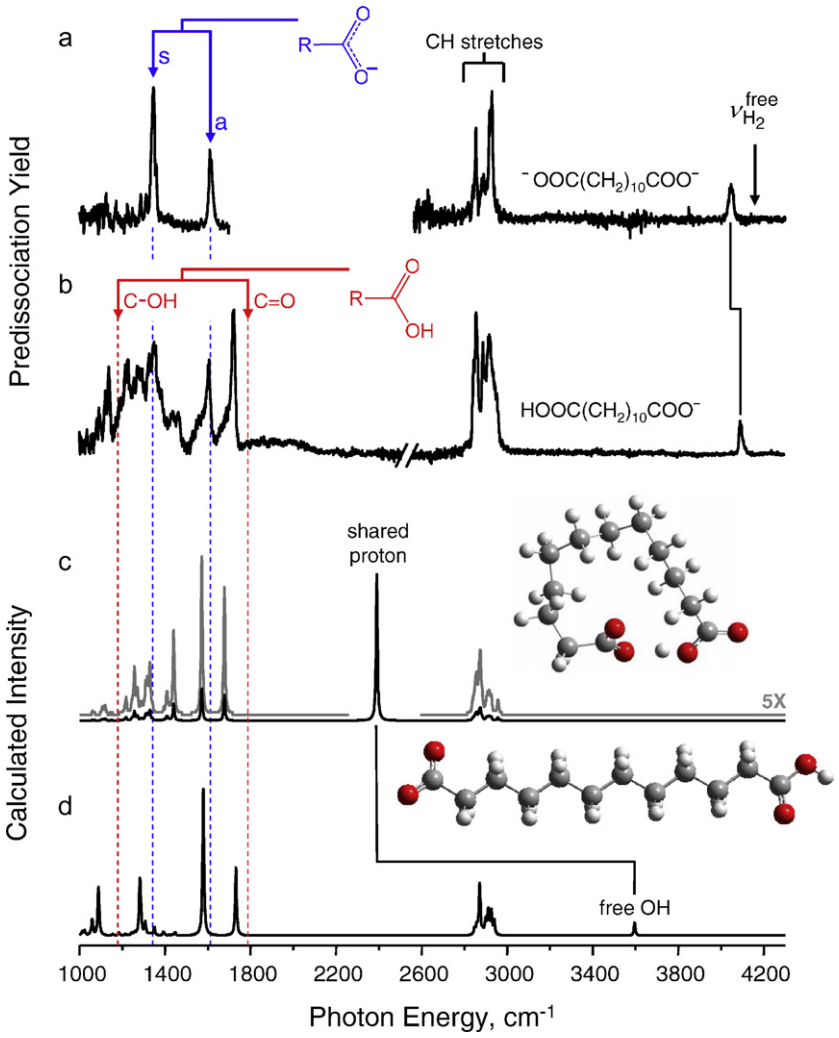

Fig. 7. Vibrational predissociation spectra (a) $^{-}OOC(CH_2)_{10}COO^{-}$ $(H_2)_{10}$ and (b) $HOOC(CH_2)_{10}COO^{-}$ $(H_2)_2$. Band positions of the carboxylate moiety in the dianion are highlighted by arrows in (a), while the positions of the two C–O stretches in neutral acetic acid are highlighted in (b). Calculated harmonic spectra (B3LYP/6-311++G(d,p)) of $HOOC(CH_2)_{10}COO^{-}$ for the (c) cyclic and (d) linear isomers. Because of the dominant intensity of the band associated with the shared proton, the gray trace in (c) presents an expansion (×5) to facilitate comparison with the experimental spectrum in (b). Calculated frequencies have been scaled by 0.956 as described in the text.

4. Conclusions

We report the vibrational spectra of the $^{-}OOC(CH_2)_{10}COO^{-}$ and $HOOC(CH_2)_{10}COO^{-}$ ions over the range 800–4300 cm^{-1}. The ions were generated by deprotonation of dodecanedioic acid in an electrospray ion source, and the spectra were obtained by predissociation of weakly bound H_2 molecules, which were attached to the ions by pulsing a H_2/He mixture into a cryogenically cooled ion trap held at a temperature varied over the range 10–20 K. The photofragmentation behavior establishes that the H_2 molecules are bound by about 600 cm^{-1}, and calculations indicate that H_2 induces very little perturbation to the geometries or spectra of the anions to which it is attached. The observed H_2 bands fall quite close to that of neutral H_2, and are more redshifted when complexed to the doubly charged species than when bound to the singly charged ion. This effect is traced to the formation of an intramolecular H-bonded ring structure in the singly charged form, which acts to disperse the excess charge across the donor and acceptor moieties. The behavior of the C–O stretches suggest that the intramolecular H-bond is asymmetrical, consistent with the calculated minimum energy structure in which the asymmetry in the ring causes the two carboxylate groups to adopt different chemical environments when tethered by a shared proton.

Acknowledgements

We thank the Air Force Office of Scientific Research under grant FA-9550-09-1-0139 for support of this work, and acknowledge extensive discussions with Profs. Xuebin Wang and Lai-Sheng Wang on the implementation of the cold Paul trap. We also greatly appreciate advice from Profs. Scott Anderson and Thomas Rizzo on the design of ion guides for efficient transmission through differentially pumped regions.

Appendix A. Supplementary data

Optimized geometries of the various conformations of the dianions and their calculated relative energies. Supplementary data associated with this article can be found, in the online version, at doi:10.1016/j.ijms.2010.10.021.

References

[1] M.F. Bush, R.J. Saykally, E.R. Williams, Evidence for water rings in the hexahydrated sulfate dianion from IR spectroscopy, J. Am. Chem. Soc. 129 (2007) 2220–2221.
[2] K. Rajabi, K. Theel, E.A.L. Gillis, G. Beran, T.D. Fridgen, The structure of the protonated adenine dimer by infrared multiple photon dissociation spectroscopy

and electronic structure calculations, J. Phys. Chem. A 113 (2009) 8099–8107.
[3] R.C. Dunbar, D.T. Moore, J. Oomens, IR spectroscopic characterization of intermediates in a gas-phase ionic reaction: the decarbonylation of Co^+(acetophenone), Int. J. Mass Spectrom. 265 (2007) 182–186.
[4] D.R. Carl, T.E. Cooper, J. Oomens, J.D. Steill, P.B. Armentrout, Infrared multiple photon dissociation spectroscopy of cationized methionine: effects of alkali-metal cation size on gas-phase conformation, Phys. Chem. Chem. Phys. 12 (2010) 3384–3398.
[5] C.M. Leavitt, J. Oomens, R.P. Dain, J. Steill, G.S. Groenewold, M.J.V. Stipdonk, IRMPD spectroscopy of anionic group II metal nitrate cluster ions, J. Am. Soc. Mass Spectrom. 20 (2009) 772–782.
[6] L. Jiang, T. Wende, R. Bergmann, G. Meijer, K.R. Asmis, Gas-phase vibrational spectroscopy of microhydrated magnesium nitrate ions $[MgNO_3(H_2O)_{1-4}]^+$, J. Am. Chem. Soc. 132 (2010) 7398–7404.
[7] M.J. Frisch, G.W. Trucks, H.B. Schlegel, G.E. Scuseria, M.A. Robb, J.R. Cheeseman, J.J.A. Montgomery, T. Vreven, K.N. Kudin, J.C. Burant, J.M. Millam, S.S. Iyengar, J. Tomasi, V. Barone, B. Mennucci, M. Cossi, G. Scalmani, N. Rega, G.A. Petersson, H. Nakatsuji, M. Hada, M. Ehara, K. Toyota, R. Fukuda, J. Hasegawa, M. Ishida, T. Nakajima, Y. Honda, O. Kitao, H. Nakai, M. Klene, X. Li, J.E. Knox, H.P. Hratchian, J.B. Cross, V. Bakken, C. Adamo, J. Jaramillo, R. Gomperts, R.E. Stratmann, O. Yazyev, A.J. Austin, R. Cammi, C. Pomelli, J.W. Ochterski, P.Y. Ayala, K. Morokuma, G.A. Voth, P. Salvador, J.J. Dannenberg, V.G. Zakrzewski, S. Dapprich, A.D. Daniels, M.C. Strain, O. Farkas, D.K. Malick, A.D. Rabuck, K. Raghavachari, J.B. Foresman, J.V. Ortiz, Q. Cui, A.G. Baboul, S. Clifford, J. Cioslowski, B.B. Stefanov, G. Liu, A. Liashenko, P. Piskorz, I. Komaromi, R.L. Martin, D.J. Fox, T. Keith, M.A. Al-Laham, C.Y. Peng, A. Nanayakkara, M. Challacombe, P.M.W. Gill, B. Johnson, W. Chen, M.W. Wong, C. Gonzalez, J.A. Pople, Gaussian 03, Revision C.02, Gaussian, Inc., Wallingford, CT, 2004.
[8] T.S. Zwier, Laser probes of conformational isomerization in flexible molecules and complexes, J. Phys. Chem. A 110 (2006) 4133–4150.
[9] M.A. Johnson, Vibrational predissociation ion spectroscopy, in: Encyclopedia of Mass Spectrometry, vol. 5, 2002.
[10] M. Okumura, L.I. Yeh, J.D. Myers, Y.T. Lee, Infrared spectra of the cluster ions $H_7O_3^+ \cdot H_2$ and $H_9O_4^+ \cdot H_2$, J. Chem. Phys. 85 (1986) 2328–2329.
[11] T. Pankewitz, A. Lagutschenkov, G. Niedner-Schatteburg, S.S. Xantheas, Y.T. Lee, Infrared spectrum of $NH_4^+(H_2O)$: evidence for mode specific fragmentation, J. Chem. Phys. 126 (2007) 074307.
[12] D.A. Wild, P.S. Weiser, E.J. Bieske, A. Zehnacker, The $^{35}Cl^- - H_2$ and $^{35}Cl^- - D_2$ anion complexes: infrared spectra and radial intermolecular potentials, J. Chem. Phys. 115 (2001) 824–832.
[13] C. Emmeluth, B.L.J. Poad, C.D. Thompson, G.H. Weddle, E.J. Bieske, Infrared spectra of the $Li^+ \cdot (H_2)_n$ (n = 1–3) cation complexes, J. Chem. Phys. 126 (2007) 204309.
[14] N. Solca, O. Dopfer, Microsolvation of the phenol cation (Ph^+) in nonpolar environments: infrared spectra of $Ph^+ \cdot L_n$ (L = He, Ne, Ar, N_2, CH_4), J. Phys. Chem. A 105 (2001) 5637–5645.
[15] N. Solca, O. Dopfer, Protonated benzene: IR spectrum and structure of $C_6H_7^+$, Angew. Chem. Int. Ed. 41 (2002) 3628–3631.
[16] P.D. Carnegie, A.B. McCoy, M.A. Duncan, I.R. Spectroscopy, Theory of $Cu^+(H_2O)Ar_2$ and $Cu^+(D_2O)Ar_2$ in the O–H (O–D) stretching region: fundamentals and combination bands, J. Phys. Chem. A 113 (2009) 4849–4854.
[17] G.E. Douberly, A.M. Ricks, P.v.R. Schleyer, M.A. Duncan, Infrared spectroscopy of gas phase $C_3H_5^+$: the allyl and 2-propenyl cations, J. Phys. Chem. 128 (2008), 021102/021101-021102/021104.
[18] A. Fujii, T. Sawamura, S. Tanabe, T. Ebata, N. Mikami, Infrared dissociation spectroscopy of the OH stretching vibration of phenol rare-gas Van-der-Waals cluster ions, Chem. Phys. Lett. 225 (1994) 104–107.
[19] A. Fujii, E. Fujimaki, T. Ebata, N. Mikami, Infrared spectroscopy of CH stretching vibrations of jet-cooled alkylbenzene cations by using the "messenger" technique, J. Chem. Phys. 112 (2000) 6275–6284.
[20] Y. Inokuchi, R. Matsushima, Y. Kobayashi, T. Ebata, Ion core structure in $(N_2O)_n^+$ (n = 2–8) studied by infrared photodissociation spectroscopy, J. Chem. Phys. 131 (2009) 044325.
[21] M. Okumura, L.I. Yeh, J.D. Myers, Y.T. Lee, Infrared-spectra of the solvated hydronium ion-vibrational predissociation spectroscopy of mass-selected $H_3O^+ \cdot (H_2O)_N \cdot (H_2)_M$, J. Phys. Chem. 94 (1990) 3416–3427.
[22] M. Okumura, L.I. Yeh, Y.T. Lee, Infrared-spectroscopy of the cluster ions $H_3^+ \cdot (H_2)_N$, J. Chem. Phys. 88 (1988) 79–91.
[23] T.D. Vaden, B. Forinash, J.M. Lisy, Rotational structure in the asymmetric OH stretch of $Cs^+ \cdot (H_2O) \cdot Ar$, J. Chem. Phys. 117 (2002) 4628–4631.
[24] D.J. Miller, J.M. Lisy, Hydrated alkali-metal cations: infrared spectroscopy and ab initio calculations of $M^+(H_2O)_{x=2-5}$ Ar cluster ions for M = Li, Na, K, and Cs, J. Am. Chem. Soc. 130 (2008) 15381–15392.
[25] R.A. Relph, T.L. Guasco, B.M. Elliott, M.Z. Kamrath, A.B. McCoy, R.P. Steele, D.P. Schofield, K.D. Jordan, A.A. Viggiano, E.E. Ferguson, M.A. Johnson, How the shape of an H-bonded network controls proton-coupled water activation in HONO formation, Science 327 (2010) 308–312.
[26] S.G. Olesen, T.L. Gausco, G.H. Weddle, S. Hammerum, M.A. Johnson, Vibrational predissociation spectra of the Ar-tagged $[CH_4 \cdots H_3O^+]$ binary complex: spectroscopic signature of hydrogen bonding to an alkane, Mol. Phys. 108 (2010) 1191–1197.
[27] H. Schneider, K.M. Vogelhuber, F. Schinle, J.M. Weber, Aromatic molecules in anion recognition: electrostatics versus H-bonding, J. Am. Chem. Soc. 129 (2007) 13022–13026.
[28] H. Schneider, K.M. Vogelhuber, J.M. Weber, Infrared spectroscopy of anionic hydrated fluorobenzenes, J. Chem. Phys. 127 (2007) 114311.
[29] N.L. Pivonka, C. Kaposta, M. Brummer, G. von Helden, G. Meijer, L. Woste, D.M. Neumark, K.R. Asmis, Probing a strong hydrogen bond with infrared spectroscopy: vibrational predissociation of $BrHBr^- \cdot Ar$, J. Chem. Phys. 118 (2003) 5275–5278.
[30] D.J. Goebbert, T. Wende, R. Bergmann, G. Meijer, K.R. Asmis, Messenger-tagging electrosprayed ions: vibrational spectroscopy of suberate dianions, J. Phys. Chem. A 113 (2009) 5874–5880.
[31] X.B. Wang, L.S. Wang, Development of a low-temperature photoelectron spectroscopy instrument using an electrospray ion source and a cryogenically controlled ion trap, Rev. Sci. Instrum. 79 (2008) 073108.
[32] X.B. Wang, X.P. Xing, L.S. Wang, Observation of H_2 aggregation onto a doubly charged anion in a temperature-controlled ion trap, J. Phys. Chem. A 112 (2008) 13271–13274.
[33] J.M. Headrick, J.C. Bopp, M.A. Johnson, Predissociation spectroscopy of the argon-solvated $H_5O_2^+$ "Zundel" cation in the 1000–1900 cm^{-1} region, J. Chem. Phys. 121 (2004) 11523–11526.
[34] H.K. Woo, X.B. Wang, K.C. Lau, L.S. Wang, Low-temperature photoelectron spectroscopy of aliphatic dicarboxylate monoanions, $HO_2C(CH_2)_nCO_2^-$ (n = 1–10): hydrogen bond induced cyclization and strain energies, J. Phys. Chem. A 110 (2006) 7801–7805.
[35] L.A. Posey, M.A. Johnson, Photochemistry of hydrated electron clusters $(H_2O)_n^-$ ($15 \leq n \leq 40$) at 1064 nm: size-dependent competition between photofragmentation and photodetachment, J. Chem. Phys. 89 (1988) 4807–4814.
[36] M.A. Johnson, W.C. Lineberger, Pulsed methods for cluster ion spectroscopy, in: J.M. Farrar, W.H. Saunders Jr. (Eds.), Techniques for the Study of Ion-Molecule Reactions, Wiley, New York, 1988, p. 591.
[37] P.B. O'Connor, C.E. Costello, W.E. Earle, A high voltage RF oscillator for driving multipole ion guides, J. Am. Soc. Mass Spectrom. 13 (2002) 1370–1375.
[38] R. Mathur, P.B. O'Connor, Design and implementation of a high power rf oscillator on a printed circuit board for multipole ion guides, Rev. Sci. Inst. 77 (2006).
[39] D. Gerlich, Ion-neutral collisions in a 22-pole trap at very-low energies, Phys. Scripta T59 (1995) 256–263.
[40] D. Gerlich, Inhomogeneous, RF-Fields, RF-fields – a versatile tool for the study of processes with slow ions, Adv. Chem. Phys. 82 (1992) 1–176.
[41] O.V. Boyarkin, S.R. Mercier, A. Kamariotis, T.R. Rizzo, Electronic spectroscopy of cold, protonated tryptophan and tyrosine, J. Am. Chem. Soc. 128 (2006) 2816–2817.
[42] M. Gerhards, C. Unterberg, A. Gerlach, Structure of a beta-sheet model system in the gas phase: analysis of the C=O stretching vibrations, Phys. Chem. Chem. Phys. 4 (2002) 5563–5565.
[43] J.A. Stearns, A. Das, T.S. Zwier, Hydrogen atom dislocation in the excited state of anthranilic acid: probing the carbonyl stretch fundamental and the effects of water complexation, Phys. Chem. Chem. Phys. 6 (2004) 2605–2610.
[44] Russell, D. (Ed.), N.S.R.D.N. NIST Computational Chemistry Comparison and Benchmark Database, Release 15a, April 2010, Johnson III, http://cccbdb.nist.gov/.
[45] P.J. Campagnola, L.A. Posey, M.A. Johnson, Controlling the internal energy content of size-selected cluster ions: An experimental comparison of the metastable decay rate and photofragmentation methods of quantifying the internal excitation of $(H_2O)^-_n$, J. Chem. Phys. 95 (1991) 7998–8004.
[46] W.H. Robertson, J.A. Kelley, M.A. Johnson, A pulsed supersonic entrainment reactor for the rational preparation of cold ionic complexes, Rev. Sci. Instrum. 71 (2000) 4431–4434.
[47] K.P. Huber, G. Herzberg, Molecular Spectra and Molecular Structure: IV. Constants of Diatomic Molecules, Van Nostrand Reinhold Company, New York, 1979.
[48] M.A. Duncan, Infrared spectroscopy to probe structure and dynamics in metal ion–molecule complexes, Int. Rev. Phys. Chem. 22 (2003) 407–435.
[49] J.R. Roscioli, L.R. McCunn, M.A. Johnson, Quantum structure of the intermolecular proton bond, Science 316 (2007) 249–254.
[50] S. Yaghmaei, S. Khodagholian, J.M. Kaiser, F.S. Tham, L.J. Mueller, T.H. Morton, Chelation of a proton by an aliphatic tertiary diamine, J. Am. Chem. Soc. 130 (2008) 7836.